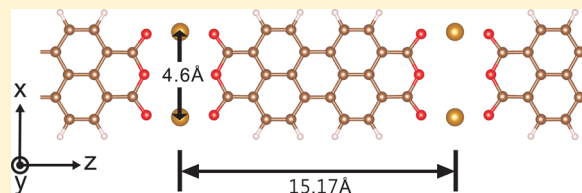


# Spin-Polarized Negative Differential Resistance in a Self-Assembled Molecular Chain

Ying-Chin Chen,<sup>†,‡</sup> Shih-Hao Hsu,<sup>†</sup> Chao-Cheng Kaun,<sup>\*,‡,¶</sup> and Minn-Tsong Lin<sup>\*,†,§</sup><sup>†</sup>Department of Physics, National Taiwan University, Taipei 10617, Taiwan<sup>‡</sup>Research Center for Applied Sciences, Academia Sinica, Taipei 11529, Taiwan<sup>¶</sup>Department of Physics, National Tsing-Hua University, Hsinchu 30013, Taiwan<sup>§</sup>Institute of Atomic and Molecular Sciences, Academia Sinica, Taipei 10617, Taiwan

**ABSTRACT:** By using first-principles calculations, we investigate the electronic structures and transport properties of a self-assembled Fe<sub>2</sub>-PTCDA chain. This experimentally observed chain can grow as long as a few tens of nanometers and our calculations suggest that it conducts as a half-metal. Spin-polarized transport properties are attributed to conducting bands of the minority spin near the Fermi energy, raised by the hybridization between orbitals of the molecule and the iron atoms, while a band gap of the majority spin exists.

Moreover, this system features a highly spin-polarized negative differential resistance, due to the alignment of conducting bands and the match of their symmetries, which can be integrated to build multifunction spintronic devices.



## INTRODUCTION

The active control and manipulation of spin degrees of freedom in molecules, namely the molecular spintronics,<sup>1</sup> is one of the promising avenues toward efficient nanoscale devices for high-density information storage and processing. To achieve a spintronic device, the most crucial issue is the generation of highly spin-polarized (SP) currents. Therefore, researchers look for molecular half-metals which have the characteristics of long spin-relaxation time/distance, pure single spin states, and distinct spin-dependent conduction behaviors. So far, pioneering theoretical works have pointed out possible materials for molecular half-metals, such as graphene nanoribbon (or carbon nanotube), modified by an external field or doped with functional groups,<sup>2–7</sup> and a transition metal–organic molecule complex.<sup>8–14</sup> However, the difficulty of patterning a circuit with the former makes that approach a challenge, whereas the latter can only be built to a few stacks<sup>15–18</sup> and is experimentally limited to short lengths, which constrains their potential applications.

In addition to the issue of experimental feasibility, understanding the spin transport behaviors of the molecular half-metals, especially in the nonlinear region, is an important step toward the device design and optimization. For instance, negative differential resistance (NDR), where the current decreases as the voltage increases, is widely used in conventional electronic devices such as frequency multipliers, memory, and fast switches.<sup>19</sup> A SPNDR device will enrich spintronics as well. While SPNDR can be generated through the spin-blockaded<sup>20</sup> or the Aharonov–Bohm effects,<sup>21,22</sup> injecting a SP current into charge-based NDR device may not produce SPNDR, because an imperfect interface can induce spin scattering and greatly lower the spin-polarization of the current

or offset other advantages.<sup>23,24</sup> A half-metal with intrinsic NDR can avoid this interface problem.

A molecular assembly is a promising candidate for nanoscale electronic and spintronic devices with novel functions,<sup>25,26</sup> as extended regular structures with different spatial dimensions can be formed.<sup>27</sup> The molecular wires, such as single chain magnets, show extra-interesting magnetic properties (e.g., soliton nucleation and kickoffs)<sup>28,29</sup> and can serve as a connecting lead or a functional device. Recently, rectangular PTCDA (perylene-3,4,9,10-tetracarboxylic-3,4,9,10-dianhydride) molecules and Fe atoms have been self-assembled on Au(111) surface to make various shapes.<sup>30,31</sup> A long molecular chain that extends to a few tens of nanometers has been grown experimentally.<sup>32</sup> While the Au substrate complicates the transport nature of the chain, these assemblies could be further transferred to (built on) dielectric substrates, where the chain–surface coupling is rather weak, for electronic and spintronic applications by using the nanoimprint (on-surface synthesis) technique.<sup>33–35</sup> Therefore, PTCDA and Fe assemblies would play important roles in both fundamental research and technical developments. However, a detailed understanding of the electronic structure and transport properties of these systems has not been addressed yet.

In this work, we theoretically explore the geometric, electronic, and transport properties of a one-dimensional Fe<sub>2</sub>-PTCDA chain and predict that the ground state of this system is half-metallic. The minority-spin metallic state around Fermi energy is produced by hybridization between the molecular orbitals (MOs) of PTCDA and the d orbitals of Fe

Received: June 17, 2014

Revised: August 18, 2014

Published: August 21, 2014

atoms. Furthermore, the calculated current–voltage ( $I$ – $V$ ) curve shows a highly spin-polarized current with a distinct NDR region. We give a clear physical picture to understanding this behavior,<sup>36,37</sup> offering an efficient way to engineer it.

## METHODS

The first-principles calculations were carried out by using spin density functional theory (DFT) within the generalized gradient approximation (GGA), in the Perdew–Burke–Ernzerhof parametrization (PBE),<sup>38</sup> for the exchange–correlation functional. The calculation was divided into two parts. In the first part, we used Quantum ESPRESSO (QE) code<sup>39</sup> to optimize atomic structures and compare the total energy of different spin configurations. All calculations were under the kinetic energy cutoffs of 46 Ry for wave functions and 370 Ry for charge density and potential. Ultrasoft pseudopotentials<sup>40</sup> were applied to represent the interaction between valence electrons and ion cores. During the relaxation, the  $1 \times 1 \times 2$  Monkhorst–Pack  $k$ -point grid was chosen to sample the Brillouin zone, while  $1 \times 1 \times 20$   $k$ -points were used for calculating total energies. After relaxation, the force acting on each atom is smaller than  $10^{-3}$  Ry/ $a_0$ . In the second part, we analyzed the electronic structure and transport properties of the system at its ground state, by using Nanodcal code,<sup>41</sup> based on DFT and nonequilibrium Green's functions formalism (NEGF). Here  $1 \times 1 \times 256$   $k$ -points were adopted to sample the Brillouin zone of the electrode. Optimized basis sets of the double- $\zeta$  with polarization (DZP) and Troullier–Martins norm-conserving pseudopotentials were employed.<sup>42</sup> Their quality was tested against the plane-wave results (band structures) of QE and good agreements were achieved. When calculating transport properties, both the left and right electrodes were semi-infinite molecular chains, while the device scattering region consisted of two unit cells of the chain. The bias voltage is applied at the edge of the scattering region, which can be achieved by gate electrodes,<sup>37</sup> causing rigid shifting of the band-structure of the leads.<sup>37,43</sup> The potential drop across the junction, calculated self-consistently, can occur since the junction current is restricted. Increasing the number of unit cells at the scattering region to four made no difference to the results. The electronic temperature was set at 300 K to stabilize calculations. The incoherent transport process, such as phonon scattering, was ignored due to the long coherence time in the molecular system.<sup>1</sup> The atomic structure and the spin-density map were plotted with the VESTA package.<sup>44</sup>

## RESULTS AND DISCUSSIONS

As shown in Figure 1, two Fe atoms with a PTCDA molecule form a unit cell, and two unit cells construct a super cell. We optimized this supercell with five possible spin configurations,

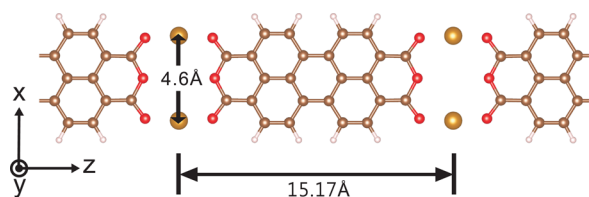


**Figure 1.** Optimized one-dimensional  $\text{Fe}_2$ –PTCDA molecular structure with a lattice constant of 15.17 Å. The Fe, C, H, and O atoms are shown in golden, brown, light gray, and red balls, respectively.

named PP, Ns, AP, PA, and AA. The first P/A denotes the spin of two nearest Fe atoms in two adjacent unit cells being parallel/antiparallel, and the second P/A indicates the spin of two Fe atoms within one unit cell being parallel/antiparallel. The Ns configuration keeps the spin of the Fe atoms in one unit cell pointing to the same direction but those in another unit cell pointing to the opposite direction. After relaxation, the Fe atoms are sandwiched in between two carboxylic oxygen atoms of adjacent PTCDA molecules and the lattice constant is close to 30.34 Å for all configurations. This molecular chain is stable, with a binding energy around  $-12.18$  eV, defined as  $E[\text{Fe}_4\text{-(PTCDA)}_2] - 2E[\text{PTCDA}] - 4E[\text{Fe}]$ , the energy difference between the chain structure and its gas-phase form (molecules and Fe atoms). However, the magnetic coupling energy contributes to the total energy and determines the ground state.

Figure 2 shows the spin density maps, arranged according to their stability. The PP configuration where all Fe atoms point to

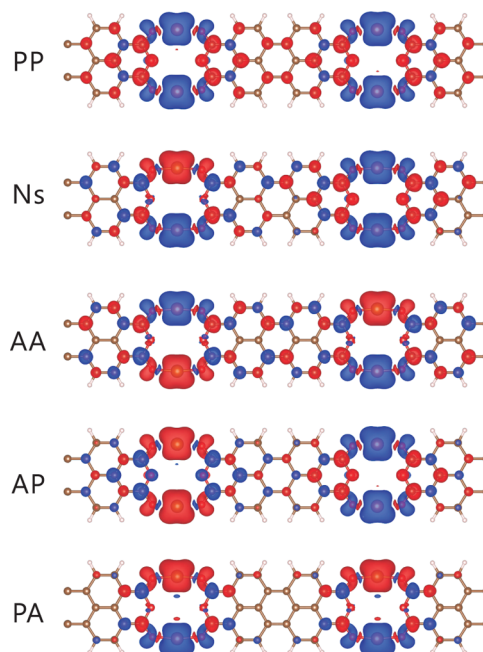


**Figure 2.** Spin-density maps ( $\rho_{\text{majority}} - \rho_{\text{minority}}$ ) of five spin configurations, arranged according to their stability, as the higher one has the lower total energy. The blue (red) color represents positive (negative) value. Isovalue =  $0.002$  e/Å<sup>3</sup>.

the same direction has the lowest total energy (20.31 meV lower than the Ns configuration), and thus is the ground state. Figure 2 also shows the magnetic couplings between the four Fe atoms, through the spin-density patterns on the PTCDA molecule and as a function of the Fe atom spin states. The absolute magnetic moment of each Fe atom has little configuration dependence, all about  $3.01 \mu_B$ . However, the spin-density patterns on PTCDA are quite different. Taking the PP state, for example, there are reflection symmetries along its horizontal and vertical central axis. Viewing along the  $z$  axis, an antiparallel spin coupling exists in each site, except at the C–C interface at the molecular center and the O–Fe interface at the molecular ends. For the Ns state, viewing along the  $z$  axis, an antiparallel spin coupling occurs in one unit cell, while another is similar to the PP state. Some C atoms have opposite spin with their surrounding atoms, resulting in little net spin

moment. Other states show different magnetic distributions which indicate rich spin behaviors of this system. Since direct coupling between Fe atoms does not occur due to the long distance, we believe that Fe atoms couple to each other via the molecules.

Since the PP state has the lowest energy, we investigate its electronic structure and transport properties. The magnetic moment per Fe atom is  $3.014 \mu_B$ , and the net magnetic moment per PTCDA molecule is  $-0.028 \mu_B$ , giving a total magnetic moment of  $6.000 \mu_B$  per unit cell. The band structure and the projected density of states (PDOS) of the majority and minority spin are shown in Figure 3, panels a and b,

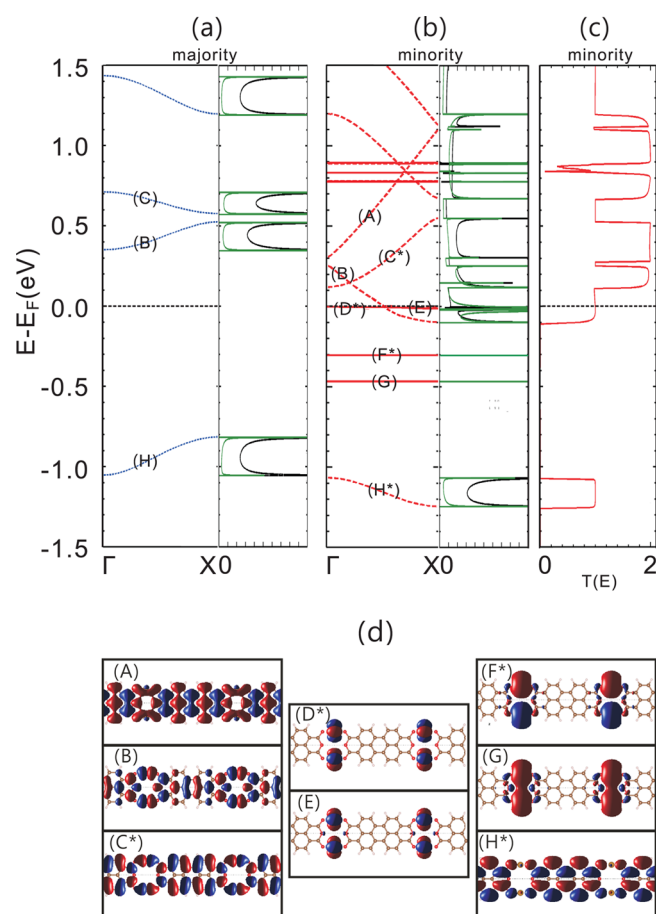


**Figure 3.** Spin-resolved electronic structures of the infinitely long  $\text{Fe}_2$ -PTCDA chain at the ground state. (a) The band structure and the projected density of states on each angular channel (p orbitals, black; d orbitals, green) for the majority spin. The flat band is represented by solid line while the sloping band is drawn with a dash line. Panel b is similar to panel a but for the minority spin. (c) The transmission spectrum of the minority spin at the zero bias. (d) The wave function at the  $\Gamma$  point of each band. Blue and red indicate opposite signs of the real part of the wave function.

respectively. Around the Fermi energy, a gap of about 1.14 eV exists for the majority electrons while a continuous PDOS occurs for the minority electrons. Both the integer number of the total magnetic moment and the band structure display the half-metallic feature. There are several PDOS peaks, resulting from the flat bands in Figure 3b, indicating that their corresponding electrons are localized. On the other hand, the sloping bands of the minority spin drawn with a dashed line in Figure 3b, contribute to the conduction and result in the

transmission spectrum shown in Figure 3c, where the number of sloping bands is equal to the number of transmission channels. We note that the localized states have little contribution to transmission even though their PDOS is high.

Figure 3d plots the eigenstates of the corresponding bands at  $\Gamma$  point. The (A) and (H) bands show the similarity as the lowest unoccupied molecular orbital(LUMO)+1 and LUMO of an isolated PTCDA molecule, respectively. In contrast, the (B) and (C) bands are new states created by the hybridization between the d orbitals of Fe and the MOs. The (D), (E), (F), and (G) bands mainly consist of d orbitals of Fe and have very small components on the molecule, which illustrate their localized nature. Based on PDOS on the p,d orbitals and the wave functions, we know that these conduction bands of the minority electrons are mainly composed of the  $p_y$  orbital of the PTCDA molecule and the  $d_{yz}$  orbital of the Fe atoms. This indicates that the hybridization between them is strong and causes a broadening of these states. On the other hand, the flat bands are formed by the  $d_{xy}$ ,  $d_{zx}$ ,  $d_{x^2-y^2}$ , and  $d_z^2$  orbitals of the Fe atoms. Therefore, near the Fermi energy the overlap of MOs and these d orbitals is weak. Their difference can be understood from the spatial shapes of the MOs and the iron d orbitals. The hybridization is mainly through the Fe–O bonds and a  $p_y$ -like orbital locates at the carboxylic oxygen. We calculated the overlap integral of  $p_y$  and all d orbitals depending on the atomic geometry. The result points out that only the iron  $d_{yz}$  orbital has a large overlap with the molecular  $p_y$  orbital, but the other four d orbitals do not. The discussion here explains the origin of the sloping/localized band. Furthermore, wave function analysis indicates that bands labeled with an asterisk have a reflection antisymmetry along its horizontal central axis, whereas other bands own a reflection symmetry. This character is important for nonequilibrium conduction properties of the chain.

From the half-metallic feature, we expect that a SP current will appear in this system, when the bias voltage is applied. The  $I$ - $V$  characteristics, shown in Figure 4a, indeed display the remarkable SP current with a NDR region. The majority-spin current is almost zero since there is no state in the applied bias window. On the other hand, the minority-spin current increases linearly as the bias voltage increases. The increasing rate slows down when the bias voltage is above 0.10 V, and the magnitude of current arrives at the maximum,  $3.00 \mu\text{A}$ , at 0.13 V. Afterward, it starts to decrease as the bias increases further. It reduces to  $1.99 \mu\text{A}$  at a bias of 0.30 V, giving a ratio of  $I_{\text{max}}/I_{\text{min}}$  of about 1.50. Finally, the current increases again, as the bias increases more.

To understand the mechanism of SPNDR, the non-equilibrium transmission spectra under bias voltages are shown in Figure 4b. Beginning from zero-bias, the conduction is dominated by the transport between the (B) band of both electrodes. One transmission channel is formed, leading to the linear dependence of the bias voltage. At 0.3 V, a gap occurs in the transmission spectrum, where the (B) band of left lead and the (C\*) band of right lead overlap. However, as the (C\*) band has an odd reflection symmetry and the (A)/(B) band has an even reflection symmetry along the horizontal central axis, the electrons cannot transport between the (B) and (C\*) bands,<sup>43,45</sup> giving a transmission gap and the  $I_{\text{min}}$ . Further increasing the bias voltage makes the (B) band of the left electrode begin to align with the (A) band of the right electrode. They are symmetry-matching states, and thus the transmission coefficients as well as the current increase again.

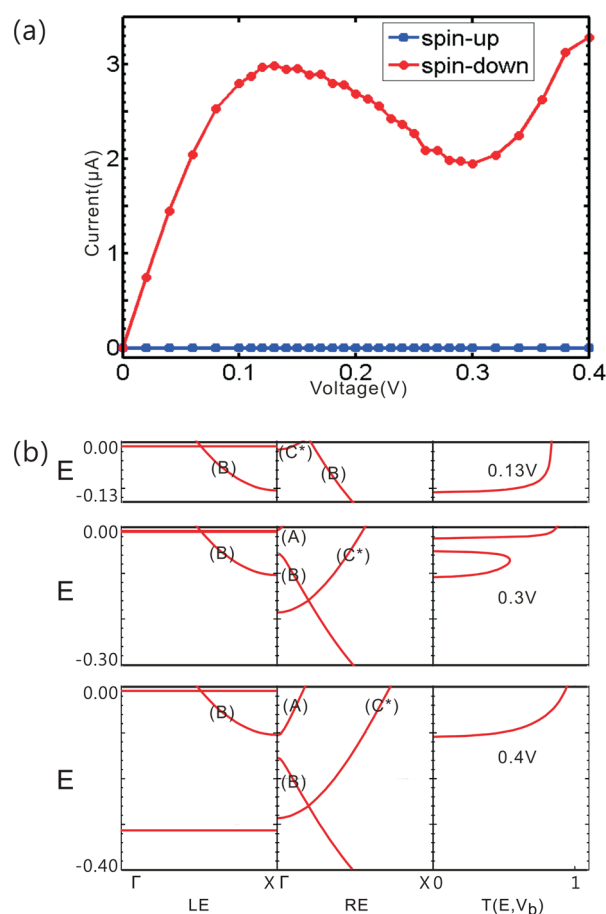


**Figure 4.** (a) Spin-polarized current–voltage characteristics. (b) The band structure of the left electrode, the band structure of the right electrode (shifted by a bias voltage), and the corresponding nonequilibrium transmission spectrum. The vertical coordinate stands for energy ( $E$ ) in units of eV and the zero-energy point is defined as the chemical potential of the left electrode.

However, the ( $C^*$ ) band can couple with the ( $A$ )/( $B$ ) band if the symmetry of wave functions is broken, for example, by applying a transverse electric field perpendicular to the transport axis.<sup>37</sup> The intrinsic and switchable features of the SPNDR effect are therefore important for future spintronic device design.

## CONCLUSIONS

In conclusion, using first-principles calculations, we suggest that the spin-polarized negative differential resistance (SPNDR) can happen in a long self-assembled molecular chain. This interesting conduction behavior is due to the half-metallicity and the match of intrinsic band symmetries in such a system. We believe that the  $\text{Fe}_2$ –PTCDA chain, with the nature of self-assembly and controllable SPNDR, is a promising candidate not only for fundamental research but also for application in molecular spintronics.

## AUTHOR INFORMATION

### Corresponding Authors

\*E-mail: kauncc@gate.sinica.edu.tw.

\*E-mail: mtlin@phys.ntu.edu.tw.

### Notes

The authors declare no competing financial interest.

## ACKNOWLEDGMENTS

This work was partially supported by the Ministry of Science and Technology, Taiwan through No. 101-2112-M-001-025-MY3 and No. 101-2120-M-002-012. The authors also thanks Dr. Nicolae Atodiresei for his helpful comments and suggestions.

## REFERENCES

- (1) Bogani, L.; Wernsdorfer, W. Molecular Spintronics Using Single-Molecule Magnets. *Nat. Mater.* **2008**, *7*, 179–186.
- (2) Son, Y.-W.; Cohen, M. L.; Louie, S. G. Half-Metallic Graphene Nanoribbons. *Nature* **2006**, *444*, 347–349.
- (3) Du, A.; Sanvito, S.; Smith, S. C. First-Principles Prediction of Metal-Free Magnetism and Intrinsic Half-Metallicity in Graphitic Carbon Nitride. *Phys. Rev. Lett.* **2012**, *108*, 197207.
- (4) Shi, X. Q.; Dai, Z. X.; Zhong, G. H.; Zheng, X. H.; Zeng, Z. Spin-Polarized Transport in Carbon Nanowires Inside Semiconducting Carbon Nanotubes. *J. Phys. Chem. C* **2007**, *111*, 10130–10134.
- (5) Hod, O.; Scuseria, G. E. Half-Metallic Zigzag Carbon Nanotube Dots. *ACS Nano* **2008**, *2*, 2243–2249.
- (6) Li, Y.; Zhou, Z.; Shen, P.; Chen, Z. Spin Gapless Semiconductor-Metal-Half-Metal Properties in Nitrogen-Doped Zigzag Graphene Nanoribbons. *ACS Nano* **2009**, *3*, 1952–1958.
- (7) Dutta, S.; Manna, A. K.; Pati, S. K. Intrinsic Half-Metallicity in Modified Graphene Nanoribbons. *Phys. Rev. Lett.* **2009**, *102*, 096601.
- (8) Maslyuk, V. V.; Bagrets, A.; Meded, V.; Arnold, A.; Evers, F.; Brandbyge, M.; Bredow, T.; Mertig, I. Organometallic Benzene-Vanadium Wire: A One-Dimensional Half-Metallic Ferromagnet. *Phys. Rev. Lett.* **2006**, *97*, 097201.
- (9) Wang, L.; Gao, X.; Yan, X.; Zhou, J.; Gao, Z.; Nagase, S.; Sanvito, S.; Maeda, Y.; Akasaka, T.; Mei, W. N.; et al. Half-Metallic Sandwich Molecular Wires with Negative Differential Resistance and Sign-Reversible High Spin-Filter Efficiency. *J. Phys. Chem. C* **2010**, *114*, 21893–21899.
- (10) Zhou, L.; Yang, S.-W.; Ng, M.-F.; Sullivan, M. B.; Tan, S.; Shen, L. One-Dimensional Iron-Cyclopentadienyl Sandwich Molecular Wire with Half Metallic, Negative Differential Resistance and High-Spin Filter Efficiency Properties. *J. Am. Chem. Soc.* **2008**, *130*, 4023–4027.
- (11) Mallajosyula, S. S.; Pati, S. K. Vanadium-Benzimidazole-Modified sDNA: A One-Dimensional Half-Metallic Ferromagnet. *J. Phys. Chem. B* **2007**, *111*, 13877–13880.
- (12) De Fusco, G. C.; Montanari, B.; Harrison, N. M. Half-metallicity in the Ferrimagnet  $\text{Nb}(\text{TCNE})_2$  from First Principles. *Phys. Rev. B* **2010**, *82*, 220404.
- (13) Da, H.; Jin, H. M.; Lim, K. H.; Yang, S.-W. Half-Metallic Spintronic Switch of Bimetallic Sandwich Molecular Wire via the Control of External Electrical Field. *J. Phys. Chem. C* **2010**, *114*, 21705–21707.
- (14) Zhu, S.; Fu, H.; Gao, G.; Wang, S.; Ni, Y.; Yao, K. A First Principles Study of Novel One-Dimensional Organic Half-Metal Vanadium-Cyclooctatetraene Wire. *J. Chem. Phys.* **2013**, *139*, 024309.
- (15) Nagao, S.; Kato, A.; Nakajima, A.; Kaya, K. Multiple-Decker Sandwich Poly-Ferrocene Clusters. *J. Am. Chem. Soc.* **2000**, *122*, 4221–4222.
- (16) Miyajima, K.; Knickelbein, M. B.; Nakajima, A. Stern-Gerlach Studies of Organometallic Sandwich Clusters. *Eur. Phys. J. D* **2005**, *34*, 177–182.
- (17) Lee, J. S.; Wang, X.; Luo, H.; Dai, S. Fluidic Carbon Precursors for Formation of Functional Carbon under Ambient Pressure Based on Ionic Liquids. *Adv. Mater.* **2010**, *22*, 1004–1007.
- (18) Zhao, X.; Ando, Y.; Liu, Y.; Jinno, M.; Suzuki, T. Carbon Nanowire Made of a Long Linear Carbon Chain Inserted Inside a Multiwalled Carbon Nanotube. *Phys. Rev. Lett.* **2003**, *90*, 187401.
- (19) Eisele, H.; Haddad, G. *Modern Semiconductor Device Physics*; Wiley: New York, NY, 1997.
- (20) Muralidharan, B.; Datta, S. Generic model for current collapse in spin-blockaded transport. *Phys. Rev. B* **2007**, *76*, 035432.

- (21) Cohen, G.; Hod, O.; Rabani, E. Constructing spin interference devices from nanometric rings. *Phys. Rev. B* **2007**, *76*, 235120.
- (22) Moldoveanu, V.; Tanatar, B. Tunable spin currents in a biased Rashba ring. *Phys. Rev. B* **2010**, *81*, 035326.
- (23) Behin-Aein, B.; Datta, D.; Salahuddin, S.; Datta, S. Proposal for an All-Spin Logic Device with Built-in Memory. *Nat. Nanotechnol.* **2010**, *5*, 266–270.
- (24) Žutić, I.; Fabian, J.; Das Sarma, S. Spintronics: Fundamentals and Applications. *Rev. Mod. Phys.* **2004**, *76*, 323–410.
- (25) Gambardella, P.; Stepanow, S.; Dmitriev, A.; Honolka, J.; de Groot, F. M. F.; Lingenfelder, M.; Gupta, S. S.; Sarma, D. D.; Bencok, P.; Stanesco, S.; et al. Supramolecular Control of the Magnetic Anisotropy in Two-Dimensional High-Spin Fe Arrays at a Metal Interface. *Nat. Mater.* **2009**, *8*, 189–193.
- (26) Klappenberger, F.; Kühne, D.; Krenner, W.; Silanes, I.; Arnau, A.; García de Abajo, F. J.; Klyatskaya, S.; Ruben, M.; Barth, J. V. Tunable Quantum Dot Arrays Formed from Self-Assembled Metal-Organic Networks. *Phys. Rev. Lett.* **2011**, *106*, 026802.
- (27) Pennec, Y.; Auwarter, W.; Schiffrin, A.; Weber-Bargioni, A.; Riemann, A.; Barth, J. V. Supramolecular Gratings for Tuneable Confinement of Electrons on Metal Surfaces. *Nat. Nanotechnol.* **2007**, *2*, 99–103.
- (28) Wernsdorfer, W.; Clérac, R.; Coulon, C.; Lecren, L.; Miyasaka, H. Quantum Nucleation in a Single-Chain Magnet. *Phys. Rev. Lett.* **2005**, *95*, 237203.
- (29) Heintze, E.; El Hallak, F.; Clau, C.; Rettori, A.; Pini, M. G.; Totti, F.; Dressel, M.; Bogani, L. Dynamic Control of Magnetic Nanowires by Light-Induced Domain-Wall Kickoffs. *Nat. Mater.* **2013**, *12*, 202–206.
- (30) Lucia, Á.; Samuel, P.; Renaud, C.; Pedro, A. S.; José, A. M.-G.; Javier, M. Metal-Organic Extended 2D Structures: Fe-PTCDA on Au(111). *Nanotechnology* **2010**, *21*, 305703.
- (31) Méndez, J.; Caillard, R.; Otero, G.; Nicoara, N.; Martín-Gago, J. A. Nanostructured Organic Material: From Molecular Chains to Organic Nanodots. *Adv. Mater.* **2006**, *18*, 2048–2052.
- (32) Yang, H.-H.; Chu, Y.-H.; Lu, C.-L.; Yang, T.-H.; Yang, K.-J.; Kaun, C.-C.; Hoffmann, G.; Lin, M.-T. Digitized Charge Transfer Magnitude Determined by Metal-Organic Coordination Number. *ACS Nano* **2013**, *7*, 2814–2819.
- (33) Chou, S. Y.; Krauss, P. R.; Renstrom, P. J. Imprint Lithography with 25-Nanometer Resolution. *Science* **1996**, *272*, 85–87.
- (34) Shevchenko, E. V.; Talapin, D. V.; Kotov, N. A.; Ó'Brien, S.; Murray, C. B. Structural Diversity in Binary Nanoparticle Superlattices. *Nature* **2006**, *439*, 55–59.
- (35) Kittelmann, M.; Rahe, P.; Nimmrich, M.; Hauke, C. M.; Gourdon, A.; Kühnle, A. On-Surface Covalent Linking of Organic Building Blocks on a Bulk Insulator. *ACS Nano* **2011**, *5*, 8420–8425.
- (36) Chen, L.; Hu, Z.; Zhao, A.; Wang, B.; Luo, Y.; Yang, J.; Hou, J. G. Mechanism for Negative Differential Resistance in Molecular Electronic Devices: Local Orbital Symmetry Matching. *Phys. Rev. Lett.* **2007**, *99*, 146803.
- (37) Li, Z.; Qian, H.; Wu, J.; Gu, B.-L.; Duan, W. Role of Symmetry in the Transport Properties of Graphene Nanoribbons under Bias. *Phys. Rev. Lett.* **2008**, *100*, 206802.
- (38) Perdew, J. P.; Burke, K.; Ernzerhof, M. Generalized Gradient Approximation Made Simple. *Phys. Rev. Lett.* **1996**, *77*, 3865–3868.
- (39) Giannozzi, P.; Baroni, S.; Bonini, N.; Calandra, M.; Car, R.; Cavazzoni, C.; Ceresoli, D.; Chiarotti, G. L.; Cococcioni, M.; Dabo, I.; et al. QUANTUM ESPRESSO: A Modular and Open-Source Software Project for Quantum Simulations of Materials. *J. Phys.: Condens. Matter* **2009**, *21*, 395502.
- (40) Rappe, A. M.; Rabe, K. M.; Kaxiras, E.; Joannopoulos, J. D. Optimized Pseudopotentials. *Phys. Rev. B* **1990**, *41*, 1227–1230.
- (41) <http://nanoacademic.ca/>.
- (42) Troullier, N.; Martins, J. L. Efficient Pseudopotentials for Plane-Wave Calculations. *Phys. Rev. B* **1991**, *43*, 1993–2006.
- (43) Kaun, C.-C.; Larade, B.; Mehrez, H.; Taylor, J.; Guo, H. Current-Voltage Characteristics of Carbon Nanotubes with Substitutional Nitrogen. *Phys. Rev. B* **2002**, *65*, 205416.
- (44) Momma, K.; Izumi, F. VESTA3 for Three-Dimensional Visualization of Crystal, Volumetric and Morphology Data. *J. Appl. Crystallogr.* **2011**, *44*, 1272–1276.
- (45) Saito, R.; Dresselhaus, G.; Dresselhaus, M. S. *Physical Properties of Carbon Nanotubes*; World Scientific: Singapore, 1998.